Manufacturability considerations in design optimisation of wave energy converters

Citation for published version:
Garcia Teruel, A & Forehand, DIM 2022, 'Manufacturability considerations in design optimisation of wave energy converters', *Renewable Energy*, vol. 187, pp. 857-873. https://doi.org/10.1016/j.renene.2021.12.145

Digital Object Identifier (DOI):
10.1016/j.renene.2021.12.145

Published In:
Renewable Energy

Manufacturability considerations in design optimisation of wave energy converters

Anna Garcia-Teruel[a,*], David I. M. Forehand[a]

[a]*Institute for Energy Systems, School of Engineering, The University of Edinburgh, Edinburgh, United Kingdom EH9 3BF*

Abstract

Wave energy converter hull shapes have been optimised in the past to find the most suitable design to maximise mean annual power production and minimise costs. However, costs are generally considered through proxies based on the device's size. When using an optimisation process capable of generating very diverse shapes, more complex objective functions may be required to ensure that resulting shapes truly minimise the levelised cost of energy. For this purpose, relevant cost factors with an effect on geometry, such as manufacturability and materials considerations, should be included in the optimisation process. To address this challenge, different strategies for incorporating manufacturability considerations in a wave energy converter optimisation process with an adaptable geometry definition are discussed here. The resulting optimal shapes are compared to the shapes obtained when these additional constraints are not included. The results show that it is possible to generate wave energy converter shapes designed for a particular manufacturing process, as well as in general with improved manufacturability characteristics - based on the shapes maximum curvature. The proposed approaches can be used in future wave energy converter design studies to generate novel and improved shapes while considering their manufacturability.

Keywords: Wave Energy Converter, Hull, Geometry, Optimization, Manufacturing, Curvature

---

*Corresponding author
Email address: `a.garcia-teruel@ed.ac.uk` (Anna Garcia-Teruel)

Nomenclature	Definition	Units
A	Submerged surface area	[m^2]
E	Coefficient of the first fundamental form	NA
f	Objective function	NA
F	Coefficient of the first fundamental form	NA
g	Equality constraint	NA
G	Coefficient of the first fundamental form	NA
h	Inequality constraint	NA
I	1st fundamental form	NA
II	2nd fundamental form	NA
L	Coefficient of the second fundamental form	NA
M	Coefficient of the second fundamental form	NA
N	Coefficient of the second fundamental form	NA
r	Radius	[m]
$\mathbf{r}_u$	Partial derivative in u of the parametric equations $\mathbf{R}(u,v)$	[-]
$\mathbf{r}_v$	Partial derivative in v of the parametric equations $\mathbf{R}(u,v)$	[-]
$\mathbf{R}(u,v)$	Vector of parametric equations	[-]
S	Surface	NA
u	Dimensionless parameter in parametric space	[-]
v	Dimensionless parameter in parametric space	[-]
v_n	Vertex	NA
V	Submerged volume	[m^3]
w	Wall thickness	[m]
$\mathbf{x}$	Vector of decision variables	NA
Δ	Solution space	NA
Ψ	Rectangular parametric space	[-]
$\kappa(\lambda)$	Curvature in direction λ	[m^{-1}]
κ_G	Gaussian curvature	[m^{-2}]
κ_1	Curvature in principal direction 1	[m^{-1}]
κ_2	Curvature in principal direction 2	[m^{-1}]
κ_{max}	Maximal absolute curvature in the principal directions	[m^{-1}]
κ_m	Mean curvature	[m^{-1}]
λ	Direction in parametric space (du, dv)	[-]
Ω	Search space	NA

Nomenclature	Definition	Units
FRP	Fibre Reinforced Polymer	NA
GA	Genetic Algorithm	NA
GRP	Glass Reinforced Polymer	NA
CFRP	Carbon Fibre Reinforced Plastic	NA
HDPE	High-Density Polyethylene	NA
NSGA-II	Elitist Non-dominated Sorting Genetic Algorithm	NA
PSO	Particle Swarm Optimisation	NA
WEC	Wave Energy Converter	NA
WES	Wave Energy Scotland	NA

1. Introduction

The geometry of Wave Energy Converter (WEC) hulls has been extensively studied in the past, due to the large potential for cost reduction associated to the structure and the importance of the hull shape for the device hydrodynamics and, therefore, power production. Geometry optimisation studies have been performed for different types of devices, which aim at maximising mean annual power production and reducing costs [1]. However, costs are represented through proxies such as device size, and relevant cost factors such as manufacturability considerations are not included in these studies.

1.1. Background

Geometry optimisation

A review of past WEC hull geometry optimisation studies was provided by Garcia-Teruel et al. [1]. For context, a few examples are provided here. A number of pre-defined geometries was compared for single-body heaving point absorbers by Goggins et al. [2], and later for sloped-motion point absorbers by Rodriguez et al. [3], which included experimental validation of the preferred shape. The effect of size depending on location was investigated by de Andres et al. [4]. Optimisation studies for single-body point absorbers were performed, for example, in [5, 6]. Other types of devices such as two-body point absorbers [7] or oscillating water columns have also been studied [8]. Although valuable insights for device design are obtained from these previous WEC geometry optimisation studies, they have mostly focused on the optimisation of devices of pre-defined shapes, such as hemispheres, or cylinders, where manufacturability considerations cannot be captured within the optimisation process, since the range of optimised solutions is limited by the geometry definition.

However, studies aiming at finding the most suitable geometry using very adaptable geometry definitions have also been performed for single-body floating WECs. The most adaptable geometry definition was presented by McCabe et al. in [9, 10], which follows an approach using B-spline surfaces for the geometry definition. The method presented in [9, 10] was extended to work for devices oscillating in any mode of motion or combination of modes of motion [11] and further implementation details to ensure the generation of feasible solutions were presented in [12]. Shapes resulting from these adaptable geometry optimisation studies could be quite complex and often had sharp edges. This would make them more challenging to manufacture, and therefore, if shapes are to be generated that truly minimise the Levelised Cost of Energy (LCOE), additional manufacturability considerations may be required. Additionally, shapes with sharp edges may result in increased vortex shedding and losses. To avoid this, curvature considerations need to be incorporated to ensure the overall improved performance of the generated shapes.

Manufacturability

Manufacturability has been considered in ship hull design for a number of years, where rolled mild steel sheets are the most widely used. Composite materials have also been used for bulkheads and moulded hulls. In 95% of these cases, Glass Reinforced Plastic (GRP) was the employed material [13]. Letcher provides an overview of different ways of defining hull geometries using B-spline surfaces, and recommends the use of developable surfaces in hull design for ease of manufacturing [14]. The use of developable surfaces in hull design was first described by Kilgore in [15] and has since been widely employed for ship hull fabrication [14]. Many recent studies have further investigated these concepts for their use in the Computer Aided Design and optimisation processes [16, 17, 18, 19].

In the wave energy sector, the main potentials and challenges regarding manufacturing and materials were already identified in 1980 by Hudson [20], with corrosion and fatigue as the main design drivers, and anti-corrosion coated steel, reinforced or pre-stressed concrete, and GRP as potential materials for the prime mover. In a more recent materials landscaping study from Wave Energy Scotland (WES) [21], potential for the development of technologies, such as adhesive bonding of composites and steel, rotational moulding of polymers, Fibre Reinforced Polymer (FRP) reinforced concrete and the use of hybrid material constructions (e.g. polymer or composite and steel hybrids, or concrete and steel hybrids) was identified. To develop these promising fields, multiple projects are ongoing as part of the WES Structural Materials and Manufacturing Processes programmes. These studies range from a feasibility test of a point absorber constructed from FRP to the development of advanced rotational moulding processes for composites. Unfortunately however, results from these projects are not yet available.

Only very few studies on manufacturability of WECs are available, among these: a study done by Pelamis [22], in which an optimised steel construction, post-tensioned concrete, and GRP were identified as possible alternatives to their initial steel design, with post-tensioned concrete giving the best results; and another study designing for buckling resistance was performed for the Sea-Wave device in [23], where Carbon Fibre Reinforced Plastic (CFRP) is identified as the most suitable material.

1.2. Goal

Given the importance of the structure for cost reduction and the ongoing efforts in development and analysis of different manufacturing processes and materials for their application in WECs, it seems fundamental to define a geometry optimisation process that considers these. The objective of WEC design optimisation should be to minimise the LCOE by considering not only generated power and device size but including relevant cost factors linked to the structure, such as manufacturability. How this can be included in a geometry optimisation process, producing meaningful results, within an acceptable time scale is discussed in this study. In particular, the inclusion of manufacturability is considered by looking at available and new promising manufacturing processes and materials, and how they constrain device geometry, through structural parameters such as curvature. Various ways of including these considerations in a WEC geometry optimisation process are demonstrated and conclusions are drawn on their suitability.

First, the general methodology used for geometry optimisation, using an adaptable geometry definition capable of generating diverse shapes is introduced in section 2. The different ways for considering manufacturability within the optimisation process are introduced as case studies in section 3. Results of these different case studies are presented in section 4. Finally, conclusions on the suitability of the different studied approaches are drawn in section 5.

2. Methodology

In this section, the general methodology used for WEC geometry optimisation is introduced. It should be noted that the present work builds on previous work by the authors. The general methodology for WEC hull geometry optimisation was discussed in detail in [12] and [24]. In the former, the suitability of the geometry definition and of the optimisation algorithm implementation were discussed. It was found that using an adaptable geometry definition versus simple geometry definitions such as a vertical cylinder, a hemisphere or a barge resulted in up to 224% higher objective function values. Using the recommended single-objective optimisation algorithms resulted in up to 11% higher objective function values while reducing computational time up to 50%. In the latter study [24], the suitability of the objective function and the problem formulation as single-objective or multi-objective were studied. It was found that single-objective optimisation results were more optimal in terms of the achieved objective function values than those obtained with the used multi-objective implementation, so that the seeding of multi-objective runs with the optimal solutions from single-objective runs was recommended. Submerged surface area based cost proxies were found to be more suitable than submerged volume based cost proxies, due to the complexity of the resulting shapes. In the present study, this previous work is extended by discussing the consideration of manufacturability in the optimisation process. In the following lines, an overview of the method will be provided for context. For more detail on the optimisation method, please, refer to [12, 24].

2.1. Optimisation problem

Both, single and multi-objective optimisation formulations are used for this study. In a single-objective optimisation problem the optimal values for a number of decision variables x_i are searched so that an objective function $f(\mathbf{x})$ is minimised or maximised. In multi-objective optimisation problems optimal solutions for a problem with various conflicting objectives ($\mathbf{f}(\mathbf{x}) = \{f_1, f_2, ..., f_n\}$) are searched, so that more than one solution will be optimal depending on the relevance of each objective function. In general, optimisation problems are formulated as minimisation problems.

A single-objective optimisation problem is represented mathematically below in the standard form [25].

$$
\begin{array}{ll}
\min f(\mathbf{x}) & \\
\text{objective function:} & f(\mathbf{x}), \quad \text{for} \quad f \in \Delta \\
\text{decision variable:} & \mathbf{x} = \{x_1, ..., x_m\} \in \Omega \\
\text{equality constraint:} & g_j(x) = 0 \quad \text{for} \quad j = 1, .., n \\
\text{inequality constraint:} & h_k(x) \leq 0 \quad \text{for} \quad k = 1, .., o
\end{array}
\tag{1}
$$

A multi-objective optimisation problem is analogously mathematically formulated as follows.

$$
\begin{array}{ll}
\min \mathbf{f}(\mathbf{x}) & \\
\text{objective functions:} & \mathbf{f}(\mathbf{x}) = \{f_1, f_2, ..., f_n\} \\
\text{decision variable:} & \mathbf{x} = \{x_1, ..., x_m\} \in \Omega \\
\text{equality constraint:} & g_j(x) = 0 \quad \text{for} \quad j = 1, .., n \\
\text{inequality constraint:} & h_k(x) \leq 0 \quad \text{for} \quad k = 1, .., o
\end{array}
\tag{2}
$$

In both cases, the full range of possible decision variable values - the search space Ω - is constrained through bounds and non-linear constraints defining restrictions between certain variable combinations. The space of feasible solutions for the studied objective function - the solution space Δ- can be constrained by various equality g_j and inequality h_k constraints. In the present study, the vector of decision variables $\mathbf{x}$ defines the WEC hull shape.

As mentioned before for single-objective optimisation, one preferred solution for a given problem will be found that minimises the objective function. On the contrary, the result of a multi-objective optimisation will be a set of solutions with objective function values that represent the best trade-off of the multiple objectives and that approximate the so called Pareto front. In this case, different solutions are commonly compared based on the Pareto dominance concept. That is, one solution is said to dominate another one, when it performs better in all or is equally good but better in at least one of the objective functions (eq. 3)

$$\forall i \in 1, ..., n : f_i(\mathbf{x}) \leq f_i(\mathbf{y}) \wedge \exists i \in 1, ..., n : f_i(\mathbf{x}) < f_i(\mathbf{y}) \tag{3}$$

A high-level overview of the optimisation process is depicted in Figure 1. The key elements of the optimisation problem are aligned with the high-level steps shown in Figure 1. These include: (1) the geometry definition through the definition of the decision variables, variable bounds and constraints; (2) the evaluation of these geometries according to the chosen objective functions; and (3) the optimisation procedure and the selected optimisation algorithms. Each of these steps, as shown in the Figure, are introduced in more detail in the consecutive subsections. Finally, methodological and theoretical aspects of including manufacturability considerations are discussed.

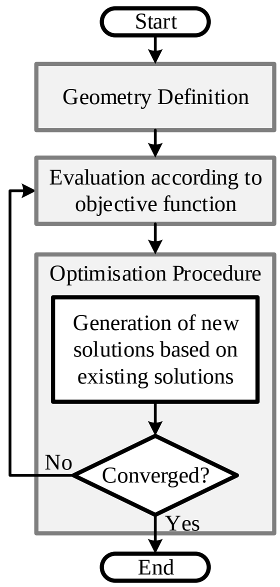

Figure 1: High-level representation of a WEC geometry optimisation process. Adapted from [26].

2.2. Geometry definition

The used geometry definition is based on the approach developed by McCabe et al. [9, 10]. This geometry definition aims at being adaptable to generate diverse shapes. It uses 11 vertices v_n of a polyhedron with an x-z-symmetry plane (see Figure 2) between which further points are interpolated using the interpolation scheme found to generate the best results in [9]. The vertices and the interpolated points are used as control points that are approximated by a bicubic B-spline surface. The coordinates of the vertices constitute the decision variables of the optimisation problem and can move randomly in space, within certain limits (the decision variable bounds). Additionally, a number of constraints are considered to ensure that the generated geometries are closed and that the B-spline surface does not cross itself. In total 22 coordinates can be varied, and, therefore, 22 decision variables are considered. Spherical coordinates (r_n, θ_n, ϕ_n) are used.

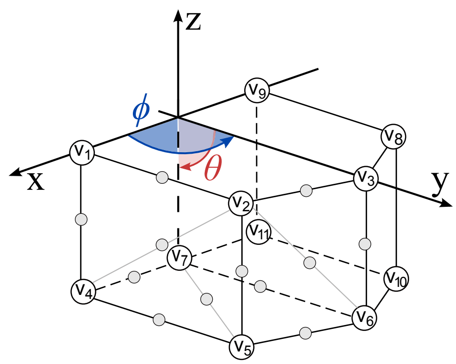

Figure 2: Geometry definition based on a polyhedron with numbered vertices v_n and vertex coordinates (r_n, θ_n, ϕ_n). Additionally, some example representations of interpolated points are shown in grey [27], adapted from Figure 1 in [10].

The considered variable bounds are listed below.

$$\begin{aligned}
2.5\text{m} \leq & r_n \leq 12.5\text{m} && \mid n = 1, .., 11 \\
-7\pi/16 \leq & \theta_n \leq -\pi/16 && \mid n = 4, 5, 6, 10, 11 \\
\pi/16 \leq & \phi_n \leq 15\pi/16 && \mid n = 3, 6 \\
\pi/16 \leq & \phi_n \leq \pi/2 && \mid n = 2, 5 \\
\pi/2 \leq & \phi_n \leq 15\pi/16 && \mid n = 8, 10.
\end{aligned}$$

The main constraints defined for the geometry are as follows:

$$\begin{aligned}
\phi_2 \leq & \phi_3 \leq \phi_8 \\
\phi_5 \leq & \phi_6 \leq \phi_{10}
\end{aligned}$$

The submerged volume range was also constrained to avoid convergence on very small or very large shapes, as in [10].

$$250\text{m}^3 \leq V \leq 4000\text{m}^3$$

157 *2.3. Evaluation according to objective function*

Geometries are assessed based on the chosen objective functions. For this study, a number of objective functions are used to be able to analyse how manufacturability considerations influence the choice of the objective function. The metrics used in the objective functions (excluding manufacturability considerations introduced in section 3) include the overall mean annual power production $\bar{P}$ to account for the device performance at a given location, and two different cost proxies based on the geometry characteristics: the submerged volume V and the submerged surface area A. Three objective functions are obtained from these metrics:

$$f_1 = -\bar{P} = f(x_1, x_2, ..., x_{22}), \tag{4}$$

$$f_2 = -\frac{\bar{P}}{V} = f(x_1, x_2, ..., x_{22}), \tag{5}$$

$$f_3 = -\frac{\bar{P}}{A} = f(x_1, x_2, ..., x_{22}). \tag{6}$$

The overall mean annual power is calculated for a location on the West Shetland shelf, 40km west of the Shetland Islands, using the scatter diagram found in [10]. The 173 different sea states with a non-zero occurrence probability are represented through irregular waves using a Bretschneider spectrum and 150 frequencies ranging from 0.02 to 3 rad/s. Hydrodynamic coefficients for each shape are obtained from WAMIT, a Boundary Element Method based software [28]. To obtain the device oscillation, a pseudo-time domain model is employed as described in [1, 11]. That is, the equation of motion is formulated in the frequency domain, considering the hydrostatic, excitation, radiation, inertia and Power Take-Off (PTO) forces. This equation is then solved at the 150 frequencies describing the various wave spectra used. The time series of the device's position and velocity in 173 irregular sea states are then calculated from the superposition of the obtained frequency-domain oscillations. Impedance matching control is assumed at the energy period T_e of each sea state, which is identified by the significant wave height H_{m0} and this energy period. Time series are obtained in order to be able to apply PTO system stroke (ξ_{MAX}) and rating ($P_{PTO,MAX}$) constraints. The overall mean annual power is then calculated by taking into account the occurrence of these different sea states. The maximum capture width (CW_{MAX}) of an axisymmetric device, calculated using the power per metre crest length P_{pm} for deep sea conditions, is used to ensure that the calculated average power per sea state $\bar{P}(H_{m0}, T_e)$ does not surpass the theoretical limit of average power available in the sea, as defined in [29]. Although the bodies considered in the present implementation are not axisymmetric, this is used as an upper bound.

$$\begin{aligned} \xi_{MAX}(i) &= 5\text{m} \quad && |\, i = 1,2,3 \\ \xi_{MAX}(i) &= \pi/4 \quad && |\, i = 4,5,6 \\ \xi_{MIN}(i) &= -\xi_{MAX}(n) \quad && |\, i = 1,2,3,4,5,6 \\ P_{PTO,MAX} &= 2.5MW && \\ 0 \text{ MW} \leq \bar{P}(H_{m0}, T_e) &\leq \text{CW}_{MAX} \cdot P_{pm} && \end{aligned}$$

The submerged volume is obtained from WAMIT. The submerged surface area is calculated following the method introduced in [24], which employs the discretised surface obtained from the low-order mesh outputted by WAMIT, which is generated from the bi-cubic B-spline surface description of the geometry.

2.4. Optimisation procedure

Meta-heuristic optimisation algorithms are used for both the single-objective and the multi-objective formulations due to their suitability to solve complex problems [1].

For the single-objective problems, both Genetic Algorithms (GAs) and Particle Swarm Optimisation (PSO) algorithms are used. GAs are based on evolution theory and emulate the survival of the fittest individuals in a population. Their implementation builds on [30]. PSO algorithms are based on the behaviour of bird flocking and fish schooling, where solutions of the optimisation problem are represented by particles moving in space. Their implementation builds on the code provided in [31]. The choice of the optimisation algorithms and their implementation is based on a previous study [12], where 14 different implementations in total were applied to a WEC optimisation problem. The same adaptable geometry definition was used for a device oscillating in surge only and in surge, heave and pitch while using different objective functions. The same combinations of Degrees-of-Freedom (DoFs) are used here as example cases to represent single and multi-DoF oscillating devices. An overview of the used implementations for the single-objective cases is provided in Table 1, where the used number of individuals N_{Ind} in the population for each iteration is provided. All optimisation problems were evaluated for 100 iterations unless convergence was reached after a minimum of 50 iterations. Convergence is defined as the objective function integer, calculated in [W] and [m], not improving for 20 iterations. Further details of the different implementations can be found in [12].

Table 1: Summary of the most suitable optimisation algorithms for the studied cases.

Objective function	**# DoFs**	Algorithm	N_{Ind}
$f_1 = -\bar{P}$	1	GA	44
	3	GA	22
$f_2 = -\frac{\bar{P}}{V}$	1	PSO	22
	3	PSO	44
$f_3 = -\frac{\bar{P}}{A}$	1	GA	44
	3	PSO	22

For the multi-objective problems, an adapted Elitist Non-dominated Sorting Genetic Algorithm (NSGA-II) algorithm is used. This is a widely used optimisation algorithm for multi-objective problems since it has proven to generate good results for a wide range of problems [32]. The implementation builds on [33]. The most suitable implementation of this algorithm for WEC optimisation using the same adaptable geometry definition was studied in [24], where it was found that using Intermidiate Recombination [34] and Breeder Genetic Algorithm mutation [34] for the recombination and mutation operators, results in better optimisation results based on the resulting Pareto Front characteristics. In this case, all of the studied cases obtained better results with the same implementation, in which the population is composed of 44 individuals, out of which 40 parents are selected for reproduction. Further details can be found in [24]. However, it should be noted here, that different objective functions were used in that study, where manufacturability was not taken into account. The use of partially different objective functions means that the solution space will be different and therefore that an additional study should be performed for a better tuning of the algorithm to the problem at hand to improve the optimality of the found solutions. This is, however, outside of the scope of this study, which focuses on demonstrating and assessing the suitability of different approaches to include manufacturability in the optimisation process. Once one of these approaches is chosen and applied to WEC hull optimisation, a study to tune the optimisation algorithm implementation should be performed.

2.5. Manufaturability considerations

With the goal of including manufacturability in a geometry optimisation process, it is important to understand how available and new promising manufacturing processes and materials constrain device geometry, through structural parameters such as curvature or hull thickness. Based on the literature reported in section 1.1, a set of materials and manufacturing processes is selected, listed in Table 2, so that a wide range of them is represented. For each of the material and manufacturing process combinations, constraints on size, wall thickness w, allowed radii r and Gaussian curvature κ_G for the part to be manufactured are collected in Table 3. If the Gaussian curvature is 0, it means that the shape is curved in only one direction - such as a rolled sheet of steel. A preliminary version of this review of materials and manufacturing processes was presented by the authors in [35].

Table 2: Selection of materials and manufacturing processes to be used for WEC's fabrication and assembly.

Material group	**Material examples**	**Manufacturing process examples**
Steel	Mild	Bending, Rolling, Welding
Concrete	Reinforced	Casting
Polymers	HDPE	Rotational moulding
Composites	GRP	Spray, Adhesive bonding
	FRP	Vacuum bag moulding, Adhesive bonding

Table 3: Manufacturing process specific constraints. The numbers in square brackets are references.

Process	w **[mm]** Min	w **[mm]** Max	r **[mm] Min**	**Size Max**	$\kappa_G \neq 0$
Bending	3 [36, 37]	150 [36]	0.5 w [38]	2x4m [36, 37]	✗
Rolling	0.13 [39]	25 [39]	2 w [39]	2x4m [36, 37]	✗
Welding [40]	3.175	-	-	-	✓
Casting [41]	-	2 w_{min} [1]	1.5 w	-	✓
Rotational moulding [42]	0.75	50	13	10m^3	✓
Spray	1.524 [43]	NA [43]	6 [44]	100m^2 [44]	✓
Vacuum bag moulding	2.032 [43]	12.7 [43]	1 [44]	20m^2 [44]	✗
Adhesive bonding [45]	$2w$+0.051 [2]	$2w$+0.254 [2]	-	-	✓

It becomes apparent that curvature, and the possibility of manufacturing parts with double curvatures (i.e. Gaussian curvature $\kappa_G \neq 0$) is the most constraining feature for both currently available processes using mild steel, and for new processes using composite materials. For this reason, the concept of curvatures in surfaces and their calculation are introduced in the following. Additionally, the minimum wall thickness will be indirectly constrained by the maximum curvature. The maximum allowed wall thickness due to the manufacturing process could be considered through the displaced mass if a percentage contribution to the total weight of ballast and equipment can be assumed.

Different strategies for including manufacturability and materials considerations in the geometry optimisation process will be evaluated here, by comparing the optimisation results to the ones obtained through an equivalent optimisation process that does not include these considerations. The different strategies are introduced in section 3.

2.5.1. Curvature definitions and calculation

Surfaces are commonly represented implicitly ($f(x, y, z) = 0$), explicitly ($z = f(x, y)$) or parametrically ($x = f(u, v), y = g(u, v), z = h(u, v)$). In con-

[1] Although no absolute wall thickness constraint was found, a constraint in the difference in wall thickness within a part exists. '*The recommended range of wall thickness is two times the thinnest wall section.*' [41]

[2] The total wall thickness will include the wall thickness of the two parts to be bonded together $2w$ and the required thickness of bonding material, taking into account an adhesive bondline thickness of 0.051 to 0.254 mm according to [45].

trast to implicit representations, the parametric surface definition supports the representation of points on the surface, enabling its polygonal description, and the analysis of its geometrical features. Compared to explicit representations it can also describe surfaces, where more than one z-value for a certain x-y-value combination exists, such as a sphere. The parametric surface definition is widely utilised in ship hull design since it can be used to describe a wide range of shapes. Therefore, an introduction to parametric surfaces based on differential geometry theory [46], the geometry of surfaces for ship hull design [14], splines [47], and Matlab based modelling of curves and surfaces [48] is given here.

In a parametric surface definition, each Cartesian coordinate (x, y, z) is expressed through two dimensionless parameters (u, v) in parametric space, for defined ranges of these parameters $u \in [a, b]$ and $v \in [c, d]$, where $x(u, v)$, $y(u, v)$ and $z(u, v)$ are continuous. Mathematically this is described as

$$\begin{aligned} &x = x(u, v), \quad y = y(u, v), \quad z = z(u, v) \\ &\text{in} \quad \Psi = (u, v) | a \leq u \leq b, c \leq v \leq d, \end{aligned} \tag{7}$$

or in matrix form

$$\mathbf{R} = \mathbf{R}(u, v) = \begin{pmatrix} x(u, v) \\ y(u, v) \\ z(u, v) \end{pmatrix} \quad \text{for} \quad (u, v) \in \Psi, \tag{8}$$

where Ψ is the rectangular parametric space, and $\mathbf{R}$ is the vector of parametric equations of surface S. A specific combination of (u, v) values can be mapped on a point on the surface S in Cartesian coordinates through the parametric equations $\mathbf{R}(u, v)$. A coordinate net on surface S is described by the u- and v-lines obtained, when the other parameter (v and u, respectively) is kept constant. These concepts are represented in Figure 3.

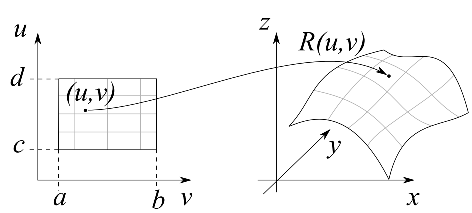

Figure 3: Representation of a parametric surface definition, with u and v-lines represented in grey [49].

From this parametric definition, various geometric properties can be found through the use of the fundamental forms [46, 48]. The 1st fundamental form is obtained from the squared arc element dS, where E, F and G are coefficients of the first fundamental form.

$$
\begin{aligned}
&I = dS^2 = (\mathbf{r}_u du + \mathbf{r}_v dv)^2 = Edu^2 + 2Fdudv + Gdv^2, \\
&\text{where} \quad \mathbf{r}_u = \frac{\partial \mathbf{R}(u,v)}{\partial u}, \mathbf{r}_v = \frac{\partial \mathbf{R}(u,v)}{\partial v}, \\
&\text{and} \quad E = \mathbf{r}_u \cdot \mathbf{r}_u, \quad F = \mathbf{r}_u \cdot \mathbf{r}_v, \quad G = \mathbf{r}_v \cdot \mathbf{r}_v.
\end{aligned} \tag{9}
$$

The surface area A of a patch on surface S corresponding to Ω in the parametric plane can be obtained with the help of this 1$^{\text{st}}$ parametric form, as in equation (10), by making use of the vector product identity $|\mathbf{r}_u \times \mathbf{r}_v| = (\mathbf{r}_u \cdot \mathbf{r}_u)(\mathbf{r}_v \cdot \mathbf{r}_v) - (\mathbf{r}_u \cdot \mathbf{r}_v)^2$.

$$
A(u,v) = \int\int_{\Omega} |\mathbf{r}_u \times \mathbf{r}_v|\, dudv = \int\int_{\Omega} \sqrt{EG - F^2} dudv. \tag{10}
$$

The 2$^{\text{nd}}$ fundamental form describes how the arc length changes with a variable t along the surface's normal vector $\mathbf{n}$. The parametric equations that describe the family of surfaces resulting from a stretch along the normal vector can be written as $\mathbf{R}(u,v,t) = \mathbf{r}(u,v) - t\mathbf{n}(u,v)$. The 2$^{\text{nd}}$ fundamental form can therefore be written as follows in equation (11), where L, M and N are the coefficients of the second fundamental form.

$$
\begin{aligned}
&II = \frac{1}{2}\frac{\partial}{\partial t}\Big(E(t)du^2 + 2F(t)dudv + G(t)dv^2\Big)|_{t=0}, \\
&\quad \text{where} \quad E(t) = \mathbf{r}_u \cdot \mathbf{r}_u, \quad F(t) = \mathbf{r}_u \cdot \mathbf{r}_v, \quad G(t) = \mathbf{r}_v \cdot \mathbf{r}_v, \\
&II = Ldu^2 + 2Mdudv + Ndv^2, \\
&\quad \text{where} \quad L = \mathbf{r}_{uu} \cdot \mathbf{n}, \quad M = \mathbf{r}_{uv} \cdot \mathbf{n}, \quad N = \mathbf{r}_{vv} \cdot \mathbf{n}, \\
&\quad \text{and} \quad \mathbf{r}_{uu} = \frac{\partial \mathbf{r}_u}{\partial u}, \quad \mathbf{r}_{uv} = \frac{\partial \mathbf{r}_u}{\partial v}, \quad \mathbf{r}_{vv} = \frac{\partial \mathbf{r}_v}{\partial v}.
\end{aligned} \tag{11}
$$

With the help of these two fundamental forms, the curvature κ of the surface in direction $\lambda = (du, dv)$ can be obtained

$$
\kappa(\lambda) = \frac{Ldu^2 + 2Mdudv + Ndv^2}{(Edu^2 + 2Fdudv + Gdv^2)}. \tag{12}
$$

Equation (12) can have two extreme values, which represent the surface's principal curvatures (κ_1 and κ_2) in the principal directions (λ_1 and λ_2).

The Gaussian curvature κ_G can be obtained from the fundamental forms or the principal curvatures:

$$
\kappa_G = \kappa_1 \cdot \kappa_2 = \frac{LN - M^2}{EG - F^2}, \tag{13}
$$

and the mean curvature κ_m is calculated as the average curvature between the two extremes

$$
\kappa_m = \frac{1}{2}(\kappa_1 + \kappa_2). \tag{14}
$$

3. Case studies

Shapes resulting from previous studies did not consider how the shapes could be manufactured, and if the available manufacturing techniques might constrain the range of feasible solutions. For this reason, different methodologies are introduced here, as example applications, for the inclusion of manufacturability considerations in the optimisation process of a WEC.

There are different strategies for including manufacturability and materials in the geometry optimisation process. On one hand, if a certain manufacturing process and material combination has been chosen, this can change how the geometry is defined or can introduce additional constraints on the optimisation variables or on the feasible resulting geometries. On the other hand, if the aim is to find an optimal geometry that can be manufactured regardless of the manufacturing process and material choice, the geometry can be checked through similar but less limiting constraints. Both these options imply constraining the geometry definition according to manufacturing limitations. This is represented in Figure 4 (a). Another option is to not only constrain the geometry but to include the price or ease of manufacturing as an objective function in the optimisation process, as shown in Figure 4 (b). This can be done by scoring the manufacturing processes and materials so that the most suitable manufacturing process aiming at cost reduction can be chosen. Hence, the result is either a multi-objective optimisation, where one objective is the manufacturability score and the second objective is the annual energy production, or a single-objective optimisation, where these two objectives are combined to represent a meaningful objective, for example as components of the LCOE.

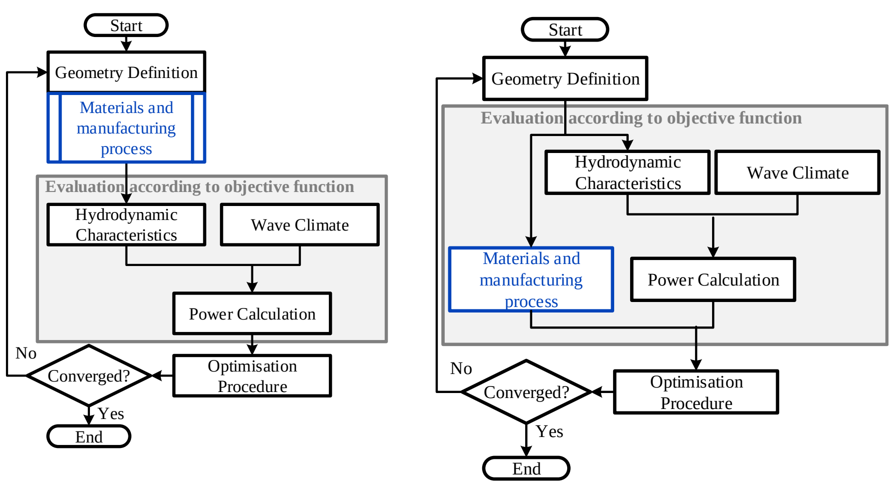

(a) (b)

Figure 4: Ways of accounting for manufacturability within a geometry optimisation process [49] (a) as a constraint, (b) as an objective function.

In the following two subsections (3.1 and 3.2), manufacturability will be considered as a constraint within the geometry definition (subsection 3.1) and as an objective function in a multi-objective optimisation (subsection 3.2). Within subsection 3.1, two approaches will be pursued: constraining the geometry to be constructed from developable surfaces and constraining the geometry's maximal curvature. In subsection 3.2, the maximal curvature will be used as one of the objective functions in a multi-objective optimisation

3.1. Manufacturability as a geometry definition constraint

As shown in Figure 4 (a), a possible strategy to include manufacturability in the optimisation process is to constraint the geometry definition itself. This is done here following two methodologies, firstly, defining the geometry to be manufacturable with a particular material and manufacturing process, and secondly, constraining the maximum curvature of the geometry.

3.1.1. Developable surfaces in the shape definition for steel manufacturing

The most limiting factor in the manufacturing of hulls out of rolled and welded steel sheets is the fact that these processes do not allow for double curvatures. It is common practice in the construction of ship hulls that the hull shape is designed to be composed of developable surfaces, which can be formed from flat steel sheets. The geometry definition is, therefore, limited here to the use of developable surfaces as a design constraint for manufacturability with steel. The resulting optimised shapes are compared to the unconstrained case.

In this study, the manufacturability-constrained geometry is split into three developable surfaces (P1, P2, P3 in Figure 5) defined through cubic-spline curves in one parametric direction and linear spline curves in the other. The same definition of the polyhedron vertices is used as introduced in section 2.2. Shapes are optimised for the ojective functions introduced in section 2.3 $f_1 = -\bar{P}$, $f_2 = -\frac{\bar{P}}{V}$ and $f_3 = -\frac{\bar{P}}{A}$. Preliminary results of this study were presented in [35].

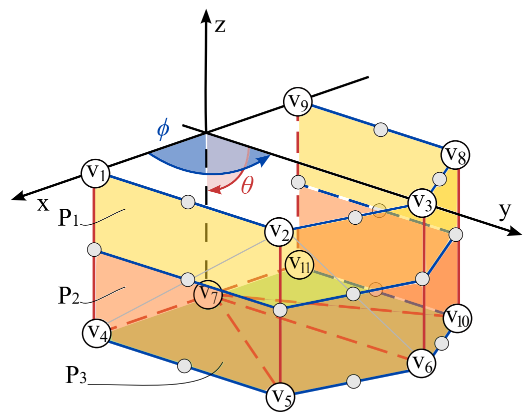

Figure 5: Geometry definition using three developable surfaces (P1, P2, P3) defined with cubic spline curves in one direction (blue) and linear spline curves in the other (red) [49].

3.1.2. Curvature as a constraint

In the previous case, the geometry was defined based on a specific manufacturing technique. In this case, the original geometry definition is used, however, a constraint on the allowed maximal curvature is applied, so that if the constraint is violated, the geometry is penalised by setting $\bar{P}$=0, V=Inf and A=Inf.

The Gaussian curvature is commonly used to describe the curvature of a surface and it can be calculated from the principal curvatures (as shown in equation (13)). However, from its definition it becomes clear that if the curvature in one of the principal directions is zero, then the Gaussian curvature is also zero.

As a result, to include curvature as a constraint, the maximal absolute value of the principal curvatures (κ_1, κ_2) across the whole surface is used, so that extreme curvatures can be avoided.

This is done by calculating the values of the principal curvatures on the surface at a number of discrete points using the parametric surface representation of section 2.5.1. The surface can be discretised into squares (in parametric space) by evaluating the surface represented by $\mathbf{R}(u, v)$ at a discrete number of equally-spaced u and v values. This was done by defining a set of vectors $\mathbf{t}_u \in [-1, 1]$ and $\mathbf{t}_v \in [-1, 1]$ with steps of size $\Delta u = \Delta v$. The maximal absolute values of the two principal curvatures at each point were mapped on the surface in Figure 6, and the run times and overall maximal absolute values for the different discretisation resolutions were recorded in Table 4. This preliminary study was performed to find the right trade-off of calculation accuracy and run time. The absolute values of the principal curvatures are taken since both convex and concave curves, corresponding to positive and negative curvatures, are considered in the optimisation process.

In Figure 6, it can be seen that both (a) ($\Delta u = 0.02$) and (b) ($\Delta u = 0.05$) are able to represent all critical high curvature locations. In Table 4, however,

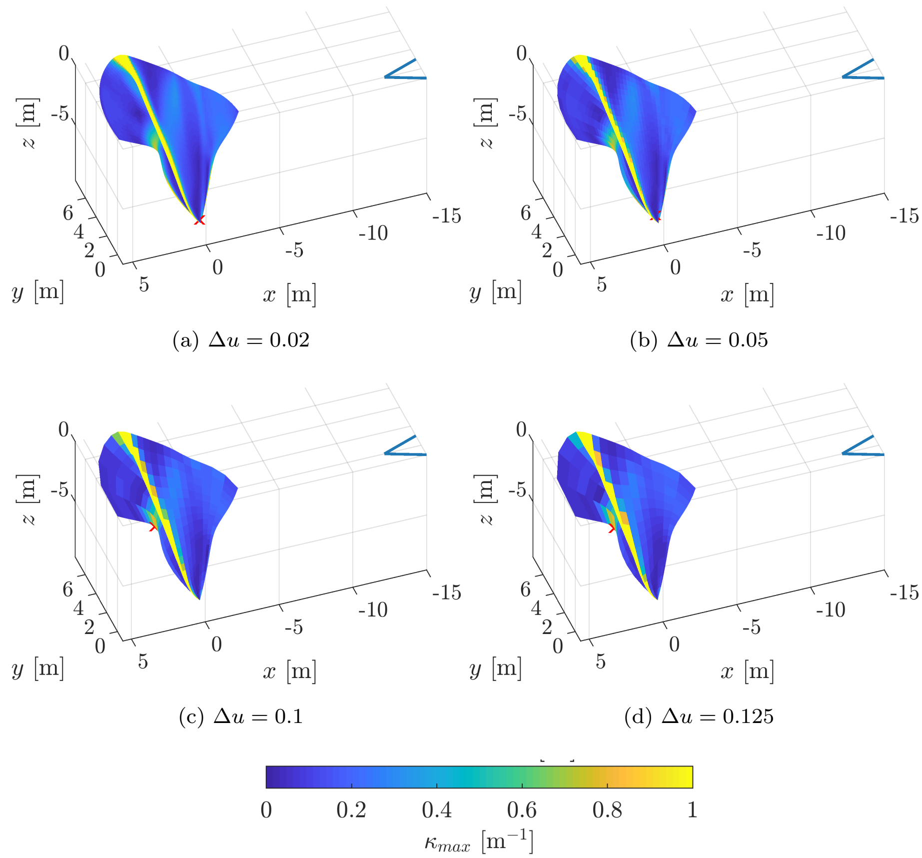

Figure 6: Half of optimal submgerged geometry with colormap reflecting the maximal absolute value of the principal curvatures at each of the surface grid points for different surface discretisation resolutions [49]. Note that the chosen range for the colormap does not include the full range of obtained curvature values in order to visualise areas of moderate to high curvatures. A red cross in each of the subfigures indicates where the highest curvature was found.

Table 4: Summary of run time and overall maximal absolute principal curvature value κ_{max} results for different resolutions of the surface discretisation.

Resolution	**Run time [s]**	κ_{max} **[m^{-1}]**
$\Delta u = 0.02$	171.670	4.78E+04
$\Delta u = 0.05$	22.959	2.44E+03
$\Delta u = 0.1$	6.185	137.665
$\Delta u = 0.125$	3.615	85.168

a large jump in calculation time can be seen when moving from $\Delta u = 0.05$ to $\Delta u = 0.02$. For this reason, a resolution of $\Delta u = 0.05$ is used for the curvature calculation. For the purpose of the present study, it is important for the high curvature locations to be recognised so that they can be avoided. The chosen option represents a good trade-off between accuracy and calculation time.

The overall maximal curvature value obtained for each geometry with this method is then compared to an externally defined maximal curvature value. The choice of this constraint could be based on the available manufacturing processes and the allowed minimal radii. Here, multiple minimal radii between 0.05 m and 0.25 m and hence, maximal absolute curvatures between 4 m^{-1} and 20 m^{-1} are chosen, to be able to evaluate the effect of this constraint on resulting shapes.

Surging-only devices are optimised to minimise the objective function $f_3 = -\frac{\bar{P}}{V}$. This objective function is used here, since it has previously resulted in the most complex shapes [11, 24] and is, therefore, suitable to study the effect of including a curvature constraint in the optimisation process.

3.2. Manufacturability as objective function

Alternatively, manufacturability can be considered as an objective function in a multi-objective optimisation.

Here, as before, the concept of curvature is employed, since it appears to be the most limiting factor for using different manufacturing processes. To include the concept of curvature in the objective function to be minimised, the overall maximal absolute value of the principal curvatures across the whole surface is used, as in section 3.1.2, so that extreme curvatures can be avoided.

Single (surging) and multi-DoF (surging, heaving and pitching) oscillating devices are considered. The overall maximal absolute curvature is minimised, together with one of the following objective functions: $f_1 = -\bar{P}$, $f_2 = -\frac{\bar{P}}{V}$ or $f_3 = -\frac{\bar{P}}{A}$. The NSGA-II algorithm with modified genetic operators, introduced in section 2.4, is employed.

4. Results

4.1. Optimal geometries using developable surfaces in the shape definition for steel manufacturing

The results of the optimisation when considering manufacturability as a constraint are presented in this section. In particular, this is done for the case in which the geometry constraint is implemented by adapting the geometry definition so that only shapes that can be manufactured from rolled sheets of steel can be generated through the optimisation. The shapes resulting from this manufacturability constrained optimisation are represented in Figures 7, 8, and 9, when using the objective functions $f_1 = -\bar{P}$, $f_2 = -\frac{\bar{P}}{V}$, and $f_3 = \frac{\bar{P}}{A}$, respectively. Note, for each of the subfigures (a) to (b) in Figures 7, 8, and 9, there are two images of the corresponding optimal submerged geometry. The left image is a view of the geometry from above the free surface and the right image is a view from below the free surface. Similar trends to the optimisation results without the manufacturability constraint can be observed (see Appendix A for shapes without manufacturability considerations). Shapes optimised to maximise power tend to more hemispherical solutions. When using submerged volume as a proxy for costs, more complex and slender shapes result, despite this manufacurability constraint. When using submerged surface area cost proxies, shapes tend to conical solutions. The fact that here, a sharp, pointed tail appears in the preferred shape for the multi-DoF case (which was also the case in the unconstrained case), indicates that further manufacturability considerations, such as curvature constraints, need to be considered within the optimisation.

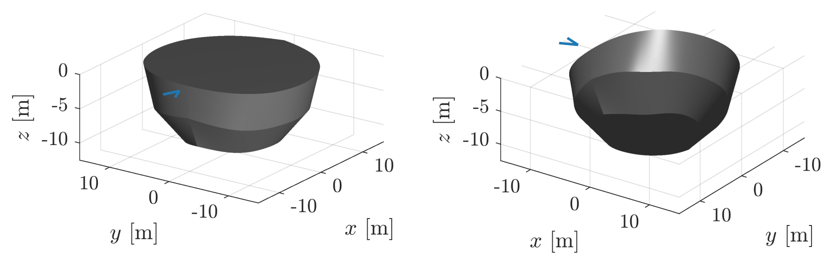

(a) $\bar{P}$, Surge

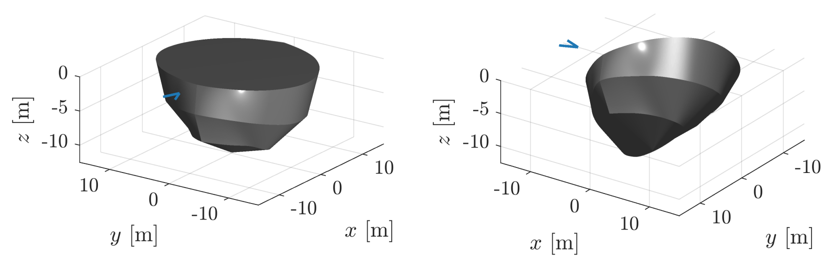

(b) $\bar{P}$, Surge, Heave and Pitch

Figure 7: Manufacturability constrained optimal geometries for WECs oscillating in surge only (a) and in surge, heave and pitch (b) optimised for $f_1 = -\bar{P}$ [49].

The mean annual power, submerged volume and submerged surface area for each of the resulting geometries are listed in Table 5 and 6, for the surging-only case, and the surging, heaving and pitching case, respectively. Similar results as obtained for the case without manufacturability constraints are achieved here. Interestingly, the $\bar{P}$ values achieved through the constrained geometries for the single-DoF cases optimised for $f_1 = -\bar{P}$ and $f_2 = -\frac{\bar{P}}{V}$ are higher than for the unconstrained case. This is because, in the former, a higher overall volume can be achieved through the modified geometry definition. In the latter, this allows for a larger cross-section perpendicular to the surging motion. In all the other cases, the larger flexibility of the unconstrained geometry definition results in higher mean annual power values.

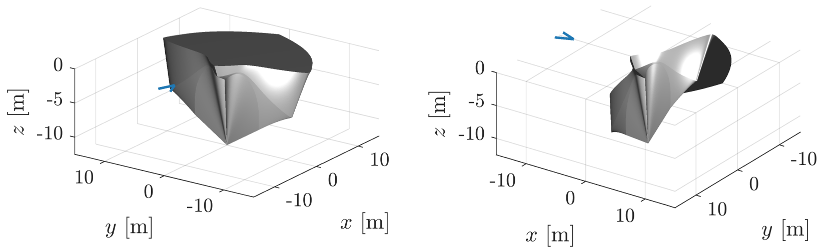

(a) $\bar{P}/V$, Surge

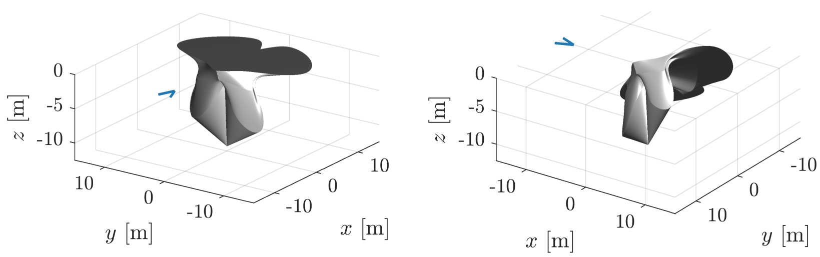

(b) $\bar{P}/V$, Surge, Heave and Pitch

Figure 8: Manufacturability constrained optimal geometries for WECs oscillating in surge only (a) and in surge, heave and pitch (b) optimised for $f_2 = -\bar{P}/V$ [49].

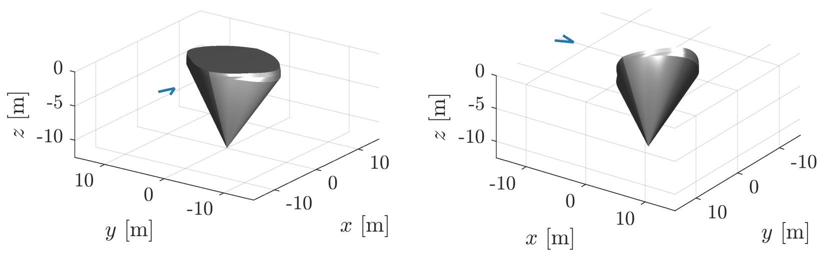

(a) $\bar{P}/A$, Surge

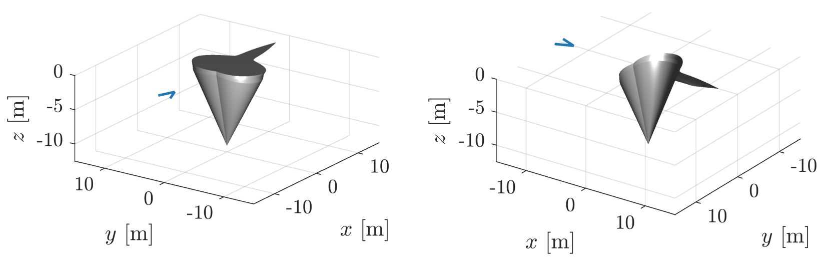

(b) $\bar{P}/A$, Surge, Heave and Pitch

Figure 9: Manufacturability constrained optimal geometries for WECs oscillating in surge only (a) and in surge, heave and pitch (b) optimised for $f_3 = -\bar{P}/A$ [49].

Table 5: Comparison of the optimisation results using developable surfaces in the shape definition (Constrained) and using the original definition proposed by McCabe [10] (Unconstrained) for a device oscillating in surge.

	Constrained			**Unconstrained**		
Objective Function	$\bar{P}$ **[kW]**	V **[m^3]**	A **[m^2]**	$\bar{P}$ **[kW]**	V **[m^3]**	A **[m^2]**
$f_1 = -\bar{P}$	365.280	3,526.107	739.860	359.890	3,426.843	875.666
$f_2 = -\frac{\bar{P}}{V}$	232.213	251.458	452.954	225.460	255.652	490.557
$f_3 = -\frac{\bar{P}}{A}$	143.454	579.003	122.500	200.232	839.501	386.109

Table 6: Comparison of the optimisation results using developable surfaces in the shape definition (Constrained) and using the original definition proposed by McCabe [10] (Unconstrained) for a device oscillating in surge, heave and pitch.

	Constrained			**Unconstrained**		
Objective Function	$\bar{P}$ **[kW]**	V **[m^3]**	A **[m^2]**	$\bar{P}$ **[kW]**	V **[m^3]**	A **[m^2]**
$f_1 = -\bar{P}$	935.589	2,645.577	670.097	954.684	2,262.850	801.101
$f_2 = -\frac{\bar{P}}{V}$	690.060	250.060	305.759	764.204	250.017	434.857
$f_3 = -\frac{\bar{P}}{A}$	367.519	250.291	52.396	505.340	250.071	175.760

Overall, the resulting shapes can be manufactured through the rolling of steel sheets. Using volume as a cost proxy still results in more complex shapes that are more difficult to manufacture, since they require very small radii of curvature and significantly varying curvatures along the developable surfaces. As had been shown in [12], $f_3 = -\frac{\bar{P}}{A}$ results in a large reduction of the mean annual power (61% lower) when compared to shapes optimised for $f_1 = -\bar{P}$.

4.2. Optimal geometries using curvature as a constraint

This section discusses the results obtained when manufacturability is represented by a constraint on the maximal absolute curvature found on the submerged hull surface. The following constraints for the maximal absolute curvature were applied: 4 m^{-1}, 8 m^{-1}, 10 m^{-1}, 15 m^{-1}, 17.5 m^{-1}, and 20 m^{-1}. The optimisation was not able to find any optimal solutions fulfilling these constraints for the first four cases. Only 12 and 9 feasible solutions over the whole optimisation process were found for $\kappa_{max} \leq 17.5$ m^{-1} and $\kappa_{max} \leq 20$ m^{-1}, respectively. Since these are not enough for the optimisation to function correctly, the number of individuals was doubled. For $\kappa_{max} \leq 10$ m^{-1} again no feasible solutions were found, and for $\kappa_{max} \leq 15$ m^{-1} only 17 feasible solutions over the whole optimisation process were generated. In the cases of $\kappa_{max} \leq 17.5$ m^{-1}, and 20 m^{-1}, 17 and no feasible solutions were generated, respectively. Based on this, it can be concluded that the curvature constraint is too restrictive in this case, so that the optimisation algorithm is not able to generate enough feasible solutions for the optimisation procedure to function. For this reason, no further results are reported on this study. However, it should be noted that here this constraint is used in combination with objective function $f_2 = -\frac{\bar{P}}{V}$, exactly because shapes of larger curvature tend to be generated to achieve lower submerged volume values and introducing this constraint was aiming at counteracting this behaviour. So although this constraint does not serve this purpose with the current optimisation formulation, this curvature constraint may still be applicable to other cases using different geometry definitions or objective functions such as $f_1 = -\bar{P}$.

4.3. Optimal geometries using manufacturability as objective function

This section presents the results obtained when the maximal absolute curvature on the submerged hull surface is considered as an objective to be minimised in a bi-objective optimisation, together with $f_1 = -\bar{P}$, $f_2 = -\frac{\bar{P}}{V}$ or $f_3 = -\frac{\bar{P}}{A}$. The Pareto fronts for each of the combinations of objective functions are represented in pairs of one (a) and multiple (b) DoF oscillating cases in Figures 10, 11 and 12. The resulting shapes at the extremes of each of the Pareto fronts and at their median are represented for each of the combination of objective functions in Figures 13, 14 and 15.

From comparison of the Pareto fronts, it can be seen that shapes within much lower curvature ranges (2 to 10 m^{-1}) result when submerged volume and submerged surface area are not accounted for in the objective functions (see Figure 10). The highest curvature values are achieved in the case where the objective function $f_2 = -\frac{\bar{P}}{V}$ is used. In particular, this is the case for the surging-only device, where shapes with curvatures of up to 800 m^{-1} are part of the Pareto front (see Figure 11 (a)). For devices oscillating in multiple DoFs, the same curvature ranges result from using submerged volume and submerged surface area in one of the objective functions (see Figures 11 (b) and 12 (b)).

Regarding the shapes, it can be seen that, apart from the surging-only case using $f_2 = -\frac{\bar{P}}{V}$, shapes do not vary much along the found Pareto fronts. This could be a sign that the algorithm is struggling to find the true Pareto front. In the surging-only cases, curvature seems to be decreased by introducing a concave surface at the bottom of the device (see Figures 13 (e) and 15 (e)). This results in a shape where curvature changes sign along one of the principal directions. This shape might require more steps to manufacture, and might, therefore, increase manufacturing complexity more than having a higher maximum curvature. This could be considered in the future for a more precise definition of manufacturability considering not only maximum curvature but also curvature sign changes. With the present implementation this should be considered when choosing from the range of solutions on the Pareto front.

Particularly in Figures 13 (b), (d), and (f), it can be observed, that although the maximal absolute curvature of the submerged surface is minimised, the transition over the symmetry plane is not smooth, and edges result on this plane. To avoid this from happening, the geometry needs to be defined so that the surface is always continuous over the symmetry plane. This is a condition that should be included in the future.

Additionally, it can be observed that the mean annual power is not strongly affected by the maximal absolute curvature value with a decrease in mean annual power of 19% for a decrease in curvature of 81% in the case where only the overall mean annual power ($f_1 = -\bar{P}$) is minimised as second objective. There are even cases when using $f_2 = -\frac{\bar{P}}{V}$ and $f_3 = -\frac{\bar{P}}{A}$ as second objectives, where the mean annual power increases with decreasing maximal absolute curvature. This means, that if representing manufacturability with maximum curvature the objective of improving manufacturability is not opposed to maximising mean annual power.

Overall, the highest curvatures result from using submerged volume in one of the objective functions, and at the symmetry plane due to lack of a continuity condition. Curvature values do not seem to have a strong impact on mean annual power. Finally, it should be noted, that although the multi-objective optimisation algorithm implementation was found to work well for similar problems, it is not tuned to the problem at hand. A more in depth comparison of different multi-objective algorithm implementations would be required for each of the studied problems, to ensure that the Pareto Front resulting from the optimisation approaches the true Pareto front.

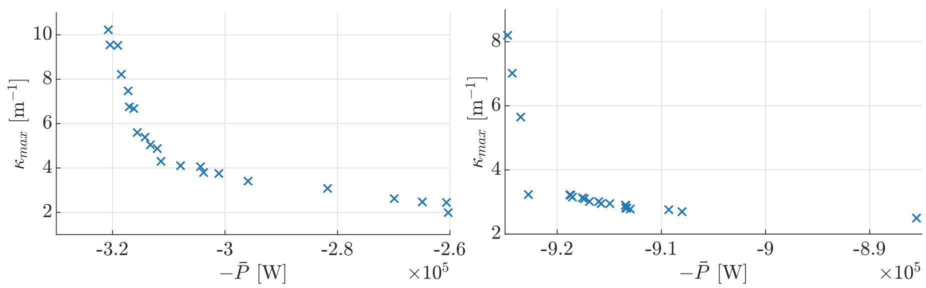

(a) Surge (b) Surge, Heave and Pitch

Figure 10: Pareto fronts for multi-objective optimisation with objective functions $-\bar{P}$ and κ_{max} [49].

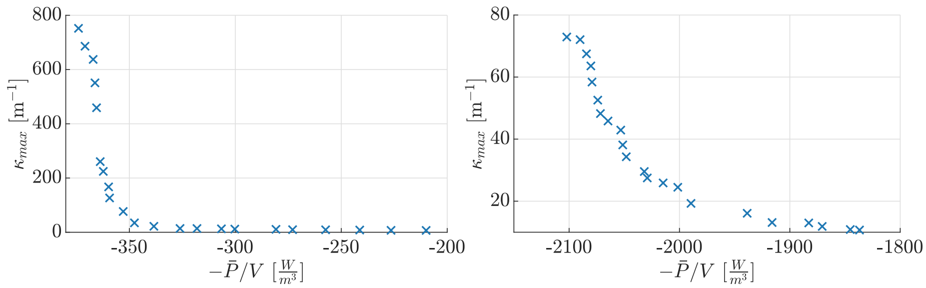

(a) Surge

(b) Surge, Heave and Pitch

Figure 11: Pareto fronts for multi-objective optimisation with objective functions $-\bar{P}/V$ and κ_{max} [49].

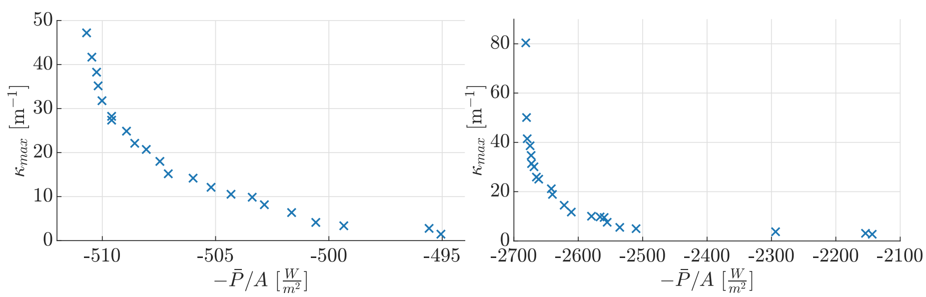

(a) Surge

(b) Surge, Heave and Pitch

Figure 12: Pareto fronts for multi-objective optimisation with objetive functions $-\bar{P}/A$ and κ_{max} [49].

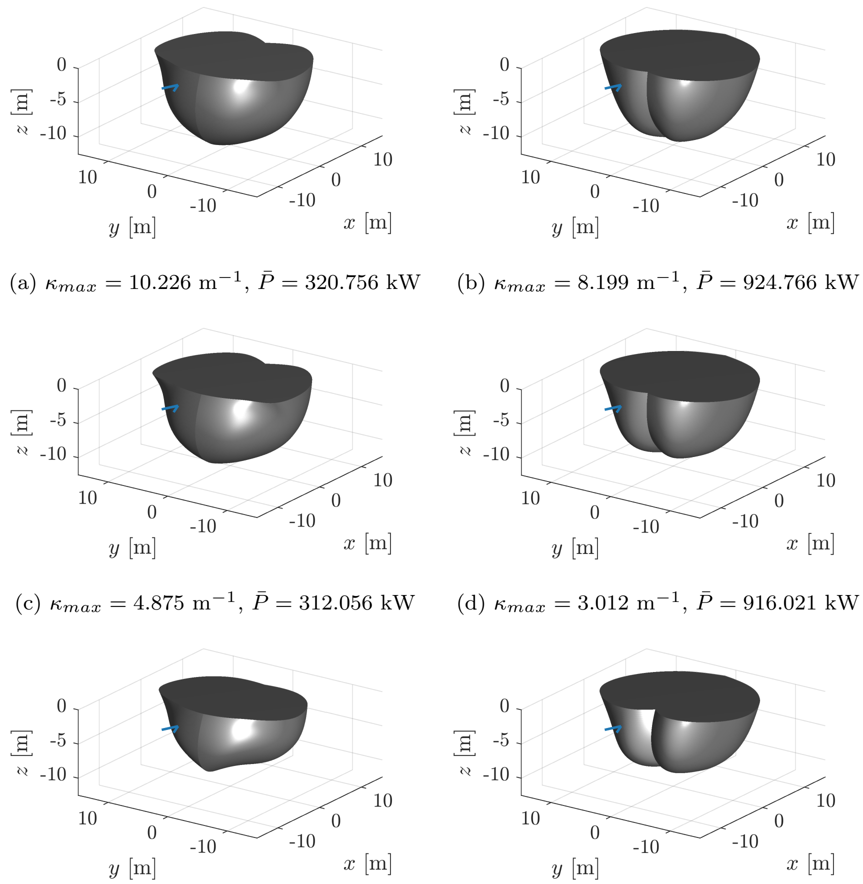

(a) $\kappa_{max} = 10.226$ m^{-1}, $\bar{P} = 320.756$ kW (b) $\kappa_{max} = 8.199$ m^{-1}, $\bar{P} = 924.766$ kW

(c) $\kappa_{max} = 4.875$ m^{-1}, $\bar{P} = 312.056$ kW (d) $\kappa_{max} = 3.012$ m^{-1}, $\bar{P} = 916.021$ kW

(e) $\kappa_{max} = 1.987$ m^{-1}, $\bar{P} = 260.304$ kW (f) $\kappa_{max} = 2.496$ m^{-1}, $\bar{P} = 885.509$ kW

Figure 13: Optimal shapes on the $\bar{P}$-κ_{max}-Pareto front for a surging-only device (a), (d) and (e), and for a surging, heaving and pitching device (b), (d), (f). (a) and (b), and (e) and (f) represent the respective Pareto front limits, and (b) and (c) represent an optimal geometry in the central area of each Pareto front [49].

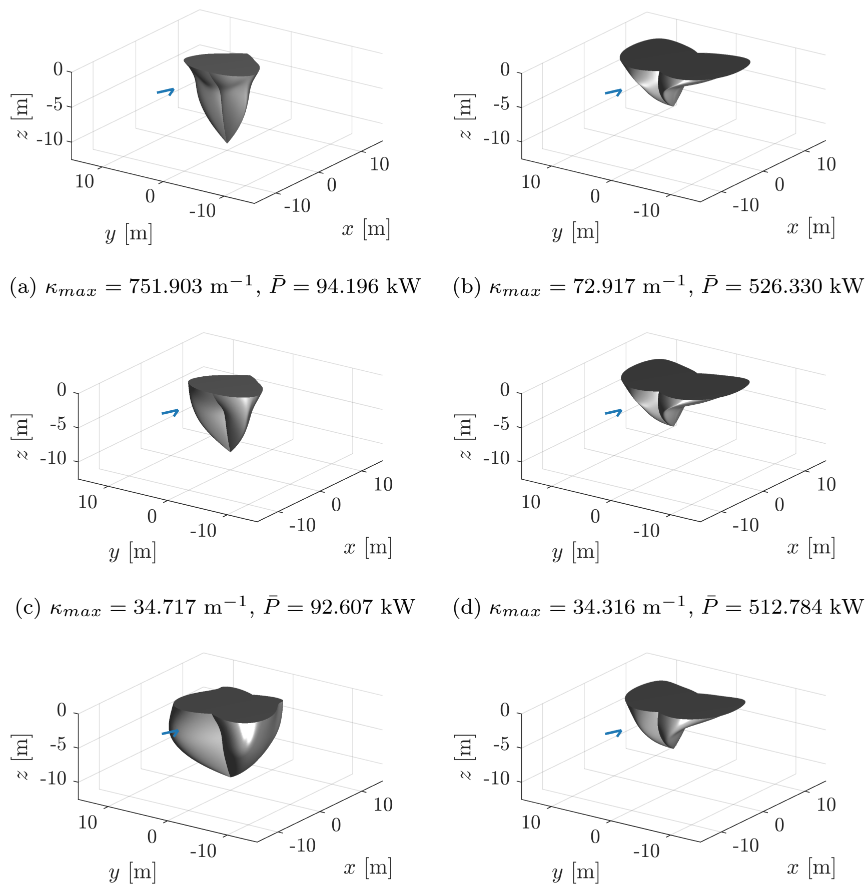

(a) $\kappa_{max} = 751.903\ \mathrm{m}^{-1}$, $\bar{P} = 94.196$ kW (b) $\kappa_{max} = 72.917\ \mathrm{m}^{-1}$, $\bar{P} = 526.330$ kW

(c) $\kappa_{max} = 34.717\ \mathrm{m}^{-1}$, $\bar{P} = 92.607$ kW (d) $\kappa_{max} = 34.316\ \mathrm{m}^{-1}$, $\bar{P} = 512.784$ kW

(e) $\kappa_{max} = 6.845\ \mathrm{m}^{-1}$, $\bar{P} = 189.174$ kW (f) $\kappa_{max} = 10.710\ \mathrm{m}^{-1}$, $\bar{P} = 484.168$ kW

Figure 14: Optimal shapes on the $\bar{P}/V$-κ_{max}-Pareto front for a surging-only device (a), (d) and (e), and for a surging, heaving and pitching device (b), (d), (f). (a) and (b), and (e) and (f) represent the respective Pareto front limits, and (b) and (c) represent an optimal geometry in the central area of each Pareto front [49].

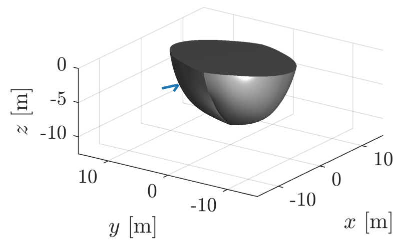

(a) $\kappa_{max} = 47.209 \text{ m}^{-1}$, $\bar{P} = 213.166$ kW

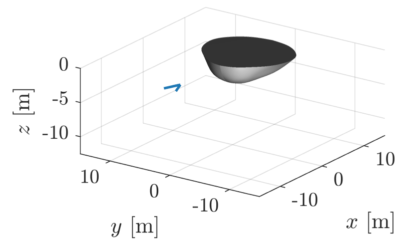

(b) $\kappa_{max} = 80.372 \text{ m}^{-1}$, $\bar{P} = 459.677$ kW

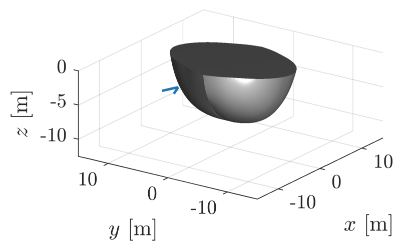

(c) $\kappa_{max} = 18.000 \text{ m}^{-1}$, $\bar{P} = 206.912$ kW

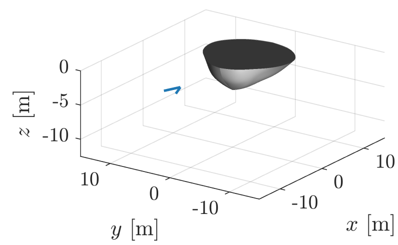

(d) $\kappa_{max} = 18.880 \text{ m}^{-1}$, $\bar{P} = 457.609$ kW

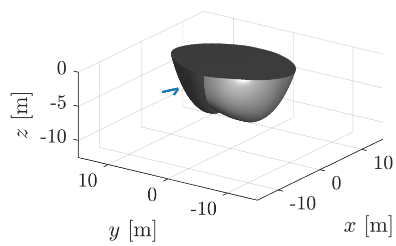

(e) $\kappa_{max} = 1.469 \text{ m}^{-1}$, $\bar{P} = 193.311$ kW

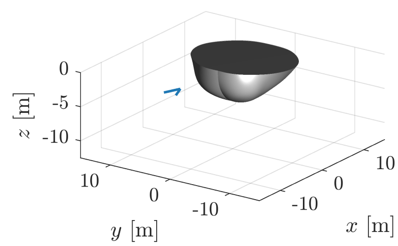

(f) $\kappa_{max} = 2.723 \text{ m}^{-1}$, $\bar{P} = 534.992$ kW

Figure 15: Optimal shapes on the $\bar{P}/A$-κ_{max}-Pareto front for a surging-only device (a), (d) and (e), and for a surging, heaving and pitching device (b), (d), (f). (a) and (b), and (e) and (f) represent the respective Pareto front limits, and (b) and (c) represent an optimal geometry in the central area of each Pareto front [49].

5. Conclusions

Manufacturability has not been previously considered in Wave Energy Converter (WEC) hull design optimisation studies. Three different ways to include manufacturability considerations in the WEC geometry optimisation process have been investigated here.

The use of developable surfaces, as performed in ship hull design for manufacturing, was studied using objective functions: $f_1 = -\bar{P}$, $f_2 = -\frac{\bar{P}}{V}$, and $f_3 = -\frac{\bar{P}}{A}$. Volume was found to not be a suitable proxy for costs, due to the more complex shapes resulting from those optimisation runs, with multiple curvatures of smaller radii, and the amount of material required depending on the surface area and not on the volume. Using rolled steel sheets as an example, it was shown that the WEC geometry can be defined specifically for the use of a given manufacturing process and material without constraining the performance of the resulting solutions. Similar approaches can be used with other manufacturing processes and materials to obtain optimised hull shapes for those cases.

To improve the results obtained with volume-based cost proxies, the use of curvature as a constraint in combination with $f_2 = -\frac{\bar{P}}{V}$ was investigated. This proved to be very limiting, even for a range of maximum absolute curvature values, so that very few feasible solutions could be generated in the optimisation process. It was, therefore, concluded that a curvature constraint is not suitable to improve the results obtained with volume-based cost proxies with the geometry definition used here. For other geometry definitions or in combination with other objective functions, a curvature constraint may still be useful to improve manufacturability of the resulting shapes.

The use of maximal absolute curvature in the objective function of a multi-objective optimisation was also studied. With this optimisation set-up, a range of solutions was generated in combination with objective functions: $f_1 = -\bar{P}$, $f_2 = -\frac{\bar{P}}{V}$, and $f_3 = -\frac{\bar{P}}{A}$, for a single and a multi-DoF oscillating device. It was found that the maximum absolute curvature value has little effect on mean annual power, and that the non-existence of a continuity condition at the symmetry plane of the hull shape resulted in some solutions having sharp edges along that plane. It was also found that multiple curvatures were introduced to reduce the value of the maximal curvature. For these reasons, for this approach to deliver consistent results it is recommended in the future to include a continuity condition at the symmetry-plane and to consider and define in more detail the optimal trade-off between smaller maximal curvatures and the number of curvatures in a given direction, which may result in additional manufacturing steps.

Although a particular geometry definition and a single-floating device was considered here, the discussed approaches to incorporate manufacturability in a WEC hull optimisation process are considered applicable to any rigid floating bodies and can be used by technology developers within their WEC design process to improve performance while reducing costs.

Acknowledgments

The authors would like to thank the Energy Technology Partnership (ETP) and UKCMER (EPSRC grants EP/I027912/1 and EP/P008682/1) for funding the Ph.D. project within which this work was performed. The authors would also like to thank Dr James Maguire for the helpful discussions on manufacturing constraints for different materials and manufacturing processes.

Appendix A. Optimal shapes for unconstrained case

The optimal shapes for the case where manufacturability was not considered in the optimisation process, as discussed in [24], are provided here for context.

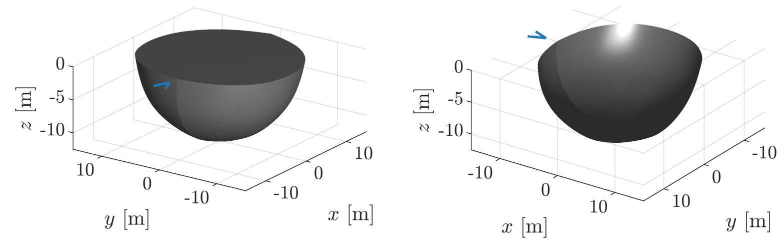

(a) P, Surge

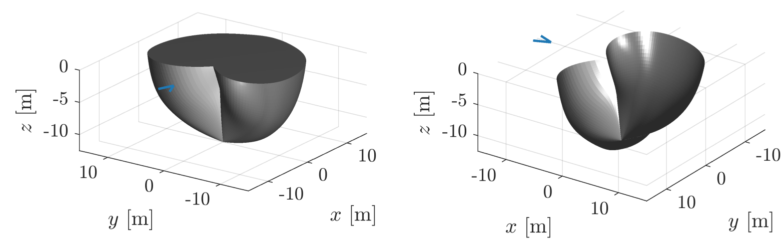

(b) P, Surge, Heave and Pitch

Figure A.16: Resulting optimal geometries for WECs oscillating in surge only (a) and in surge, heave and pitch (b) optimised for $f_1 = -\bar{P}$ when not considering manufacturability [50].

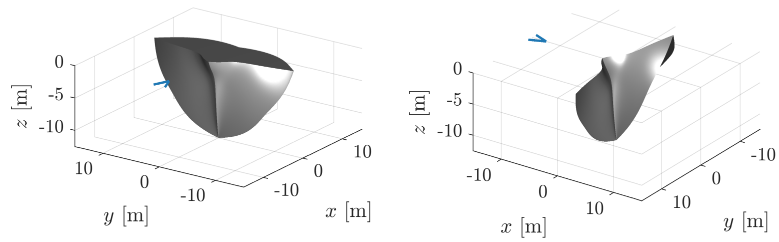

(a) $\frac{\bar{P}}{V}$, Surge

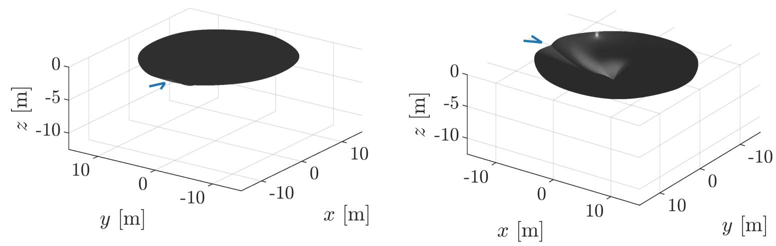

(b) $\frac{\bar{P}}{V}$, Surge, Heave and Pitch

Figure A.17: Resulting optimal geometries for WECs oscillating in surge only (a) and in surge, heave and pitch (b) optimised for $f_2 = -\bar{P}/V$ when not considering manufacturability [50].

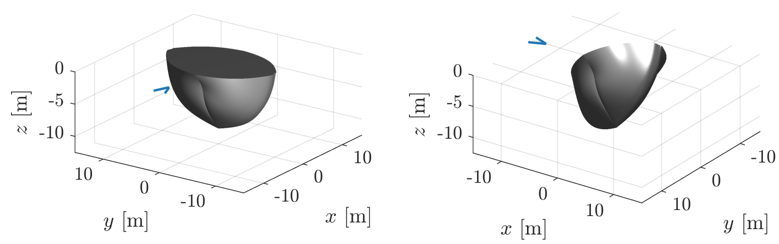

(a) $\frac{\bar{P}}{A}$, Surge

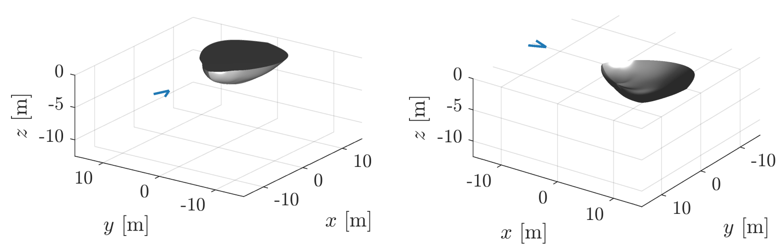

(b) $\frac{\bar{P}}{A}$, Surge, Heave and Pitch

Figure A.18: Resulting optimal geometries for WECs oscillating in surge only (a) and in surge, heave and pitch (b) optimised for $f_3 = -\bar{P}/A$ when not considering manufacturability [50].

Data availability

The data that support the findings of this study are available from the corresponding author upon reasonable request.

References

[1] A. Garcia-Teruel, D. I. M. Forehand, A review of geometry optimisation of wave energy converters, Renewable and Sustainable Energy Reviews (2021). doi:10.1016/j.rser.2020.110593.

[2] J. Goggins, W. Finnegan, Shape optimisation of floating wave energy converters for a specified wave energy spectrum, Renewable Energy 71 (2014) 208–220. doi:10.1016/j.renene.2014.05.022.

[3] C. A. Rodríguez, P. Rosa-Santos, F. Taveira-Pinto, Hydrodynamic optimization of the geometry of a sloped-motion wave energy converter, Ocean Engineering 199 (2020). doi:10.1016/j.oceaneng.2020.107046.

[4] A. de Andres, R. Guanche, C. Vidal, I. J. Losada, Adaptability of a generic wave energy converter to different climate conditions, Renewable Energy 78 (2015) 322–333. doi:10.1016/j.renene.2015.01.020.

[5] A. Babarit, A. H. Clément, Shape optimisation of the SEAREV wave energy converter, in: Proc. of the 9th World Renewable Energy Congress, 2006.

[6] A. Kurniawan, T. Moan, Multi-objective optimization of a wave energy absorber geometry, in: Proc. of the 27th International Workshop on Water Waves and Floating Bodies, no. 2, 2012, pp. 3–6.

[7] M. Blanco, M. Lafoz, D. Ramirez, G. Navarro, J. Torres, L. Garcia-Tabares, Dimensioning of Point Absorbers for Wave Energy Conversion by means of Differential Evolutionary Algorithms, IEEE Transactions on Sustainable Energy (2018) 1–9doi:10.1109/TSTE.2018.2860462.

[8] R. Gomes, J. Henriques, L. Gato, A. Falcão, Hydrodynamic optimization of an axisymmetric floating oscillating water column for wave energy conversion, Renewable Energy 44 (2012) 328–339. doi:10.1016/j.renene.2012.01.105.

[9] A. P. McCabe, G. A. Aggidis, M. B. Widden, Optimizing the shape of a surge-and-pitch wave energy collector using a genetic algorithm, Renewable Energy (12) 2767–2775. doi:10.1016/j.renene.2010.04.029.

[10] A. McCabe, Constrained optimization of the shape of a wave energy collector by genetic algorithm, Renewable Energy 51 (2013) 274–284. doi:10.1016/j.renene.2012.09.054.

[11] A. Garcia-Teruel, D. I. M. Forehand, Optimal wave energy converter geometry for different modes of motion, in: Advances in Renewable Energies Offshore: Proceedings of the 3rd International Conference on Renewable Energies Offshore (RENEW 2018), Lisbon, 2018, pp. 299–305.

[12] A. Garcia-Teruel, B. DuPont, D. I. M. Forehand, Hull geometry optimisation of wave energy converters: On the choice of the optimisation algorithm and the geometry definition, Applied Energy 280 (2020). doi:10.1016/j.apenergy.2020.115952.

[13] D. Eyres, A. Molland, H. Schneekluth, V. Bertram, R. Shenoi, A. Dodkins, D. Watson, Ship design, construction and operation, in: A. F. Molland (Ed.), The Maritime Engineering Reference Book - A Guide to Ship Design, Construction and Operation, Vol. 6, Elsevier Ltd, 2007, Ch. 9, pp. 638–727.

[14] J. S. Letcher, Geometry of Surfaces, in: J. R. Paulling (Ed.), The Geometry of Ships, Vol. I, The Society of Naval Architects and Marine Engineers, Jersey City, 2009, Ch. 4, pp. 30–46.

[15] U. Kilgore, Developable Hull Surfaces, Vol. 3, Fishing News (Books) Limited, London, 1967.

[16] G. Chiandussi, G. Bugeda, Shape variable definition with C 0 , C 1 and C 2 continuity functions, Computer methods in applied mechanics and engineering 188 (2000) 727–742. doi:10.1016/S0045-7825(99)00358-8.

[17] J.-H. Nam, S. Sohn, D. J. Singer, Estimation of geometry-based manufacturing cost of complex offshore structures in early design stage, International Journal of Naval Architecture and Ocean Engineering (3) 291–301. doi:10.2478/IJNAOE-2013-0097.

[18] G. Tampier B., M. Salas I., Hydrodynamic ship design for service conditions, Ocean Engineering 23–29doi:10.1016/j.oceaneng.2013.10.006.

[19] M. Ćurković, I. Marinić-Kragić, D. Vučina, A novel projection of open geometry into rectangular domain for 3D shape parameterization, Integrated Computer-Aided Engineering 25 (1) (2017) 1–14. doi:10.3233/ICA-170553.

[20] J. Hudson, D. Philips, N. Wilkins, Review Materials aspects of wave energy converters, Journal of Materials Science 15 (1980) 1337–1363. doi:10.1007/BF00752114.

[21] Wave Energy Scotland, Materials Landscaping Study, Tech. rep., Wave Enery Scotland Ltd (2016).

[22] C. Anderson, Pelamis WEC Main Body Structural Design And Materials Selection, Tech. rep., Ocean Power Delivery Ltd. (2003).

[23] H. R. Le, K. M. Collins, D. M. Greaves, N. W. Bellamy, Mechanics and materials in the design of a buckling diaphragm wave energy converter, Materials and Design 79 (2015) 86–93. doi:10.1016/j.matdes.2015.04.041.

[24] A. Garcia-Teruel, B. DuPont, D. I. M. Forehand, Hull geometry optimisation of wave energy converters: On the choice of the objective function and the optimisation formulation, Applied Energy, Under review (2021).

[25] P. Y. Papalambros, D. J. Wilde, Principles of Optimal Design : Modeling and Computation, Cambridge University Press, 2000.

[26] A. Garcia-Teruel, D. I. Forehand, A review of geometry optimisation of wave energy converters. doi:10.6084/m9.figshare.13370798.

[27] A. Garcia-Teruel, B. DuPont, D. I. Forehand, Hull geometry optimisation of wave energy converters: On the choice of the optimisation algorithm and the geometry definition. doi:10.6084/m9.figshare.13070234.v1.

[28] MIT, WAMIT User Manual.
URL http://www.wamit.com/manualupdate/V70_manual.pdf

[29] J. N. Newman, Marine Hydrodynamics, The Massachusetts Institute of Technology, 1977.

[30] A. Chipperfield, P. Fleming, H. Pohlheim, C. Fonseca, Genetic Algorithm Toolbox - User's Guide (1995).
URL http://codem.group.shef.ac.uk/public/GAToolbox_Documentation.pdf

[31] Constrained Particle Swarm Optimization, version 1.31.2 (2016).
URL https://uk.mathworks.com/matlabcentral/fileexchange/25986-constrained-particle-swarm-optimization

[32] K. Deb, S. Agrawal, A. Pratap, T. Meyarivan, A Fast Elitist Non-Dominated Sorting Genetic Algorithm for Multi-Objective Optimization: NSGA-II, Proc. of the 6th International Conference on Parallel Problem Solving from Nature (PPSN VI) (Springer-Verlag London) (2000).

[33] S. Baskar, S. Tamilselvi, P. Varshini, MATLAB code for Constrained NSGA II - File Exchange - MATLAB Central (2015).
URL https://uk.mathworks.com/matlabcentral/fileexchange/49806-matlab-code-for-constrained-nsga-ii-dr-s-baskar-s-tamilselvi-and-p-r-varshini

[34] H. Mühlenbein, D. Schlierkamp-Voosen, Predictive Models for the Breeder Genetic Algorithm, Evolutionary Computation 1 (1) (1993) 25–49. doi:10.1162/evco.1993.1.1.25.

[35] A. Garcia-Teruel, D. Forehand, H. Jeffrey, Wave Energy Converter hull design for manufacturability and reduced LCOE, in: Proc. of the 7th International Conference on Ocean Energy (ICOE), pp. 1–9.

[36] FRANKLIN STEEL plc, Mild Steel Plates, accessed: 2018-05-23.
URL https://www.franklinsteelplc.co.uk/steel-product-services/plate/mild-steel-plates/

[37] Steelexpress Ltd, Mild steel Sheets, mild steel plates, Floor Plates, accessed: 2018-05-23.
URL https://www.steelexpress.co.uk/structuralsteel/sheets.html

[38] R. Chandramouli, Metal Forming Lecture: Sheet metal operations - Bending and related processes, Tech. rep., National Programme on Technology Enhanced Learning (NPTEL).

[39] A. K. Swain, Design for Manufacture and Assembly (DFMA): Rolled formed section, Tech. rep., National Programme on Technology Enhanced Learning (NPTEL).

[40] D. H. Phillips, Welding Engineering, John Wiley & Sons, 2016.

[41] HCL Technologies Limited, Casting Design Guidelines, Tech. rep.
URL https://dfmpro.geometricglobal.com/files/2017/03/A-Definitive-Guide-to-DFM-success-Issue-II.pdf

[42] R. J. Crawford, J. L. Throne, Rotational molding technology, Elsevier Science, New York. doi:10.1016/B978-188420785-3.50005-8.

[43] Molded Fiber Glass Companies, Technical Design Guide for FRP Composite Products And Parts, Tech. rep.

[44] P. Ball, Manufacturing Processes, in: Handbook of Polymer Composites for Engineers, Woodhead Publishing Ltd, 1979, Ch. 2, pp. 73–98. doi:10.1016/0378-3804(79)90022-6.

[45] E. M. Petrie, The fundamentals of adhesive joint design and construction: Function-specific construction is the key to proper adhesion and load-bearing capabilities, Metal Finishing (11) 55–57. doi:10.1016/S0026-0576(08)80314-5.

[46] A. Pressley, Elementary Differential Geometry, 2nd Edition, Springer, 2010. doi:10.1007/978-1-84882-891-9.

[47] E. V. Shikin, A. I. Plis, Handbook on Splines for the User, CRC Press, 1995.

[48] V. Rovenski, Modeling of Curves and Surfaces with Matlab, Springer, 2011. doi:10.1007/978-0-387-74995-2.

[49] A. Garcia-Teruel, D. I. Forehand, Manufacturability considerations in design optimisation of wave energy converters. doi:10.6084/m9.figshare.18551267.

[50] A. Garcia-Teruel, B. DuPont, D. I. Forehand, Hull geometry optimisation of wave energy converters: On the choice of the objective functions and the optimisation formulation. doi:10.6084/m9.figshare.14721213.v1.